Rubio,P., Muñoz-Abella, B., Rubio,L. (2017).Neural approach to estimate the stress intensity factor ofsemi-elliptical cracks in rotating cracked shafts in bending. *Fatigue & Fracture of Engineering Materials & Structures*, 41(3), pp.539–550.

DOI: https://doi.org/10.1111/ffe.12717

Neural approach to estimate the stress intensity factor of semi-elliptical cracks in rotating cracked shafts in bending

P. Rubio B. Muñoz-Abella L. Rubio

Department of Mechanical Engineering, Universidad Carlos III de Madrid, Avda Universidad 30, 28911 Leganés, Madrid, Spain

Correspondence
P. Rubio, Department of Mechanical Engineering, Universidad Carlos III de Madrid, Avda Universidad 30, 28911 Leganés, Madrid, Spain.
Email: prubio@ing.uc3m.es

Funding information
Spanish Ministerio de Economía y Competitividad, Grant/Award Number: DPI2009-13264, DPI2013-45406-P

Abstract

In the last decades, neural network approach has often been used to study various and complex engineering problems, such as optimization or prediction. In this paper, a methodology founded on artificial neural networks (ANNs) was used to calculate the stress intensity factor (SIF) in different points of the front of a semi-elliptical crack present in a rotating shaft, taking into account the shape and depth of the crack, the angle of rotation, and the location of the point in the front. In the event of rotating machines, such as shafts, it is crucial to know the SIF along the crack front because this parameter, according to the Paris Law, is related to the performance of the crack during its propagation. Previously, it was necessary to achieve the data for the ANN training, for this a quasi-static numerical model was made, which simulates a rotating cracked shaft with a semi-elliptical crack. The numerical solutions cover a wide range of crack depths and shapes, and rotation angles. The values of the SIF estimated by the ANNs were contrasted with other solutions available in the literature finding a good agreement between them. The proposed neural network methodology is an alternative that offers a very good option for the SIF estimation, because it is efficient and easy to use, does not require high computational costs, and can be used to analyse the propagation of cracks contained in rotating shafts by means of the Paris Law taking into account the nonlinear behaviour of the shaft.

KEYWORDS

breathing mechanism, neural networks, rotating cracked shafts, semi-elliptical cracks, stress intensity factor

1 INTRODUCTION

The propagation of fatigue cracks in shafts is a very impor-tant fault that can occur in rotating machines because they can produce serious damage with considerable dangers for people and expensive maintenance actions. The shafts perform in rotation, and owing to rotating bending loads, cyclic stress is generated that produces compression and

Nomenclature: a, depth of the crack; b, neuron bias; f, activation function; h, distance from the intersection point of the ellipse with the shaft to the centre of the shaft; w, distance from any point of the crack front to the centre of the shaft; w_i, neuron weights; D, diameter of the shaft; E, Young's Modulus; F_I, nondimensional SIF; I_i, neuron inputs; K_I, stress intensity factor in mode I; L, length of the shaft; O, neuron output; MSE, mean squared error; $\alpha = \frac{a}{D}$, relative crack depth; $\beta = \frac{a}{b}$, crack shape factor; $\gamma = \frac{w}{h}$, relative position on the crack front; θ, angle of rotation; $\theta_{o\gamma}$, first rotation angle, for a given γ, in which F_I is positive; $\theta_{c\gamma}$, last rotation angle, for a given γ, in which F_I is positive; ν, Poisson ratio; ρ, density; σ, maximum reference stress

tensile stresses taking place for each rotation. Under these conditions, the shaft can fail because of the apparition and propagation of fatigue cracks. During a whole rotation of the shaft, the elliptical crack can open and close. Several researchers in the past used different ways to model the closing and opening of the crack. Some of them took into consideration that the crack is permanently open.[1,2] Other researchers considered that the crack is completely open or completely closed; therefore, the crack is open in half rotation, and the crack is closed in the other half.[3-8] This model was called "switching crack model" and has been used many times because it is very simple. Another model is the "breathing crack" one. In this model, the crack closes and opens gradually in a rotation, depending on if there are compression or tensile stresses. The transition between these states produces the partial closing or opening of the crack. Many authors also studied this model.[9-20]

On the other hand, to study the propagation of cracks due to fatigue, it is very important to determine the stress intensity factor (SIF), owing to the crack growth rate depends on the increment of the SIF in the well-known Paris-Erdogan Law. This parameter describes the stress state at the crack front. The closing and opening of the crack are related to the values of the SIF at the crack front as the shaft rotates. In the case of open crack, the SIF at the crack front is positive (tensile stresses); reversely, in the case of closed crack, the SIF is not positive (compressive stresses). In this sense, the SIF along the crack front in round bars has been studied by many researchers. At the beginning, many studies assumed that the crack had straight front.[21-25] This configuration has been usually used. However, the real fatigue cracks usually have fronts with semi-elliptical shape, other researches considered these kind of cracks, among them.[26-31]

The breathing mechanism of the crack occurs when a cracked shaft rotates. Some authors determined the SIF along the crack in rotating shafts taking into account the partial closing and opening of the crack, but they did not contemplate the nonlinear behaviour of the crack.[32,33] During a rotation, the crack opens and closes in a gradual way; consequently, the shaft behaviour becomes nonlinear.[10,12-14,17,18] Rubio et al[34] developed an analytical model that provides the SIF in any point of the front of a semi-elliptical crack contained in a rotating shaft taking into account the breathing mechanism and the nonlinear behaviour of the crack.

In the last 2 decades, many researchers have used artificial neural networks (ANNs) to solve a great variety of complex engineering problems, as pattern recognition, optimization, or prediction.[35-40] Artificial neural networks are computational systems inspired by biological neural networks formed by different layers: an input layer, one or more hidden layers, and an output layer. The layers involve different nodes that are connected by weights. The ANN learns the input/output relationship through a training. Artificial neural networks have been applied in crack identification inverse problems.[39-41] Similarly, some prediction models (linear or nonlinear) have been recently developed.[35,36,38,42] Moreover, ANNs have been used to determine the SIF in cracked shafts. Muñoz-Abella et al[37] used a neural network to predict the SIF in the case of a cracked unbalanced rotating shaft subjected to bending loads. The authors took into account several parameters such as the angle of rotation, the size of the crack, and the position of the eccentricity, but they did not consider the elliptical crack shape.

In this paper, an ANN to obtain the SIF a semi-elliptical crack in a rotating cracked shaft is presented. The input data used by the net are the crack size, the crack shape, the position of the point on the crack front, and the output value given by the ANN is the SIF in that point of the crack front. One of the advantages of the proposed ANN is that the methodology considers the nonlinear behaviour of the crack during a shaft rotation. This is possible because the ANN training values (input and output) were obtained from a numerical analysis developed by the commercial finite element code ABAQUS, which takes into account the breathing mechanism in the cracked section. In summary, the described system would allow studying the complex dynamic performance of cracked shafts to predict the remaining life of the element through the deeper understanding of crack propagation process.

2 | MODEL OF THE CRACKED SHAFT

The model selected for this study is a shaft of aluminium with the mechanical properties of a linear elastic material: density $\rho = 2800\,\text{kg/m}^3$, Young's Modulus $E = 72\,\text{GPa}$, and Poisson's ratio $\nu = 0.33$. The geometrical properties are diameter $D = 20\,\text{mm}$ and length $L = 900\,\text{mm}$. The shaft contains a semi-elliptical crack, with depth a (Figure 1A), which is positioned in the midspan. In Figure 1B, it can be seen that the shaft is subjected to 2 concentrated loads that have been situated at a distance $\frac{L}{4}$ from the ends of the shaft to have a pure bending conditions.

The SIF was analysed in terms of the following variables:

- Relative crack depth (depth ratio) $\alpha = \frac{a}{D}$. The crack depths chosen for the study were $\alpha = 0.1, 0.2, 0.25, 0.3, 0.4$, and 0.5 (see Figure 2A).
- Crack shape factor (shape ratio) $\beta = \frac{a}{b}$. Five crack shapes were considered $\beta = 0, 0.25, 0.5, 0.75$, and 1. The value of $\beta = 0$ corresponds to straight crack fronts and the value $\beta = 1$ to semi-circular ones.

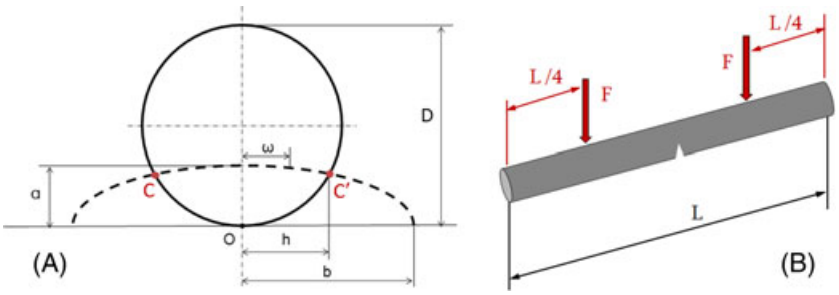

FIGURE 1 Geometric model. A, Transversal section of a shaft with a crack of elliptical front. B, Crack and loads locations [Colour figure can be viewed at wileyonlinelibrary.com]

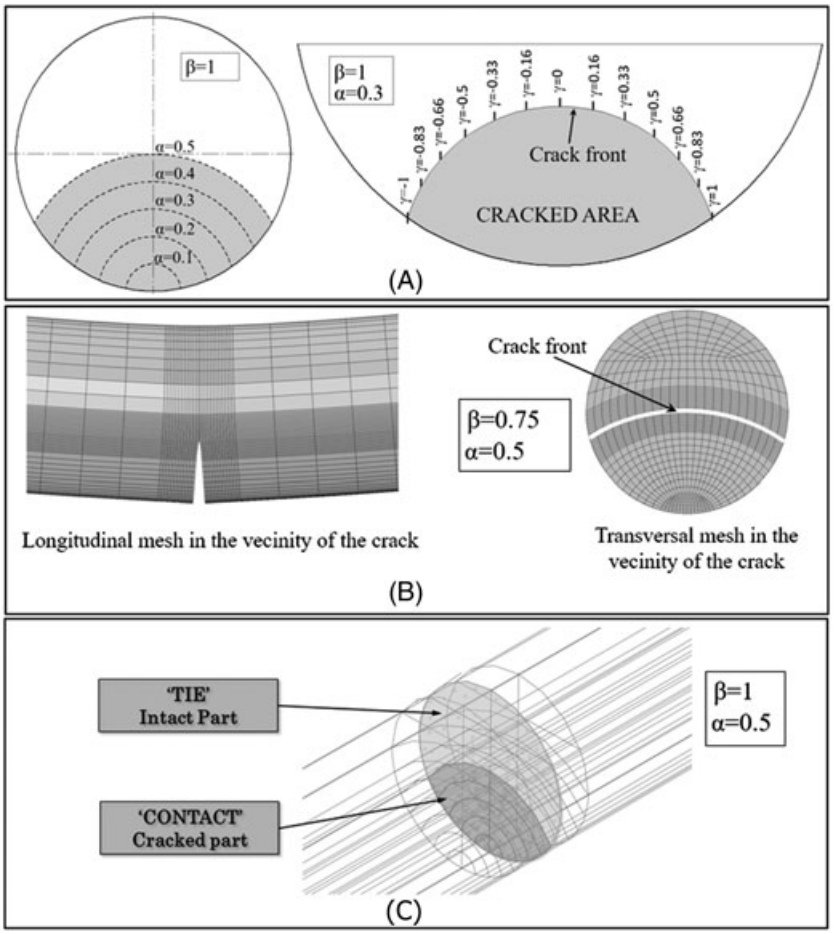

FIGURE 2 A, Different crack depths for a circular crack ($\beta = 1$) and different positions on the crack front. B, Detail of the meshed model. C, Detail of the contact interaction

- Relative position on the crack front $\gamma = \frac{w}{h}$. Eleven relative positions on the crack front γ were considered, which varies from -1 to 1 in increments of 0.16 (see Figure 2A). The positions on the end points ($\gamma = -1$ and $\gamma = 1$) were not considering in the study because at the intersection points, the singularity power depends on the intersection angle and Poisson's ratio[27,43-45] and it is not $-1/2$.
- Rotation angle θ. The behaviour of the shaft was studied considering diverse angular positions, which varies from 0 to 2π with increments of $\frac{2\pi}{72}$ (corresponding to 5°). Therefore, the SIF was evaluated at 72 angles of rotation. The shaft rotates in a clockwise direction.

2.1 | Numerical model

The finite element code ABAQUS[46] was used to carry out the numerical study. A 3D quasi-static model shaft with a crack was made with the purpose to obtain the SIF in diverse points of the crack front. The shaft was subjected to rotary bending. For the model, 8-node linear elements of reduced integration, denominated C3D8R in the

ABAQUS/standard nomenclature, were used to create the finite element mesh. The mesh was refined in the vicinity of the crack. In Figure 2B, for the case $\alpha = 0.5$ and $\beta = 0.75$ the mesh of the model is shown. A total number of 79 500 finite elements and 168 081 nodes were used, and the size of the smallest mesh element used at the crack front was $667{\cdot}10^{-3}{\times}671{\cdot}10^{-3}{\times}333{\cdot}10^{-3}\text{mm}^3$. To simulate the crack, 2 parts of the shaft were joined using the interaction "Tie," in accordance with the nomenclature of ABAQUS, between the surfaces corresponding to the uncracked section. The cracked part was defined by contact interaction called "surface to surface" in ABAQUS. The following properties of the contact interaction were selected: "hard contact," in accordance with the nomenclature of ABAQUS, as normal behaviour, which avoids that the crack faces interpenetrate when the crack closes, and "rough friction," following the nomenclature of ABAQUS, as tangential behaviour, that does not allow the relative movement between the 2 crack faces. This contact interaction can be seen in Figure 2C. Light grey zone corresponds to the uncracked section. The SIF was obtained using the module "crack" of ABAQUS, which is a specific module for fracture mechanics that allows evaluating the J-integral (J) and determining the SIF. First of all, ABAQUS determines the J-integral values, and then, for plane strain, ABAQUS calculates the SIF distribution along the crack front directly according to

$$K_I = \sqrt{J\bar{E}}, \tag{1}$$

where K_I is the SIF for mode I and $\bar{E}$ is expressed as

$$\bar{E} = \frac{E}{1-\nu^2}. \tag{2}$$

2.2 | Determination of the SIF

In conformity with the explanations that can be found in the previous sections, the SIF K_I was obtained in all cases, and from it, the nondimensional SIF F_I was calculated, according to

$$F_I = \frac{K_I}{\sigma\sqrt{\pi a}}, \tag{3}$$

where a is the depth of the crack and σ is the reference stress, calculated as the maximum bending stress of the undamaged shaft. In Figure 3A, an example of the results of the nondimensional SIF versus the position on the crack front γ is shown for the case $\alpha = 0.5\beta = 0$ and 3 rotation angles ($\theta = 0, \frac{\pi}{2}$, and π).

We can see that when the crack is fully open ($\theta = \pi$), the F_I is positive. Otherwise, if the crack is closed ($\theta = 0$), the F_I is negative. Finally, if the crack is partially open ($\theta = \frac{\pi}{2}$), the SIF passes from positive values to negative

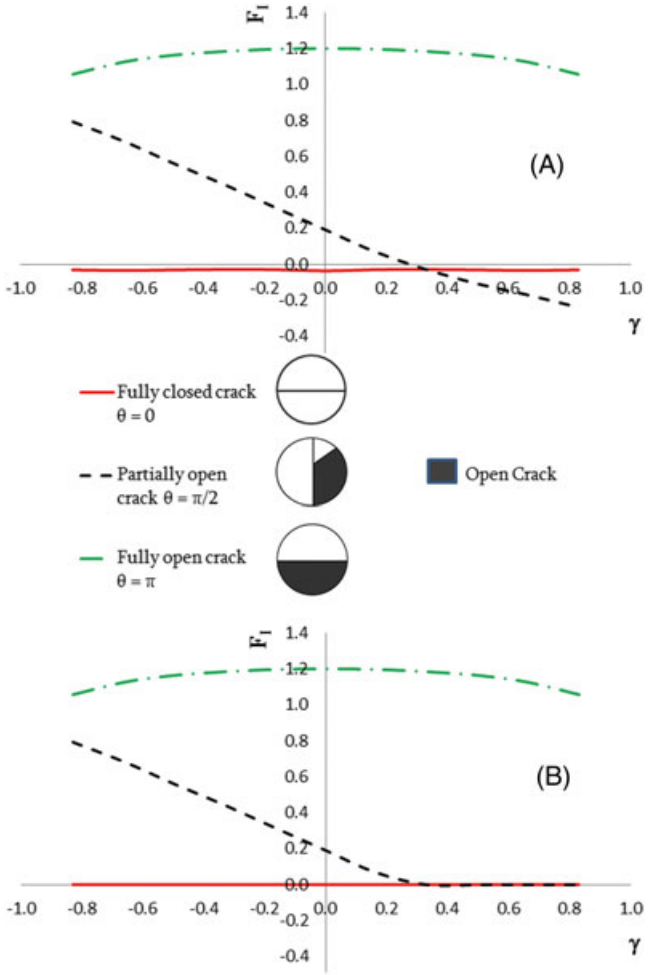

FIGURE 3 Nondimensional stress intensity factor (SIF) of the finite element method model versus location on the front γ for $\alpha = 0.5, \beta = 0$ and 3 rotation angles ($\theta = 0, \frac{\pi}{2}$, and π). A, Negative SIF values when the crack is closed. B, Null SIF values when the crack is closed [Colour figure can be viewed at wileyonlinelibrary.com]

ones. The instant when the SIF value changes from positive to negative allows identifying the position on the crack front in which the crack closes. However, according to the work presented by Rubio et al,[34] while the crack is closed, SIF values must be null, because the crack is situated in compression zone and the shaft behaves like an uncracked shaft, so negative SIF values were replaced by zero. Figure 3B shows the results of the nondimensional SIF versus the position on the crack front γ, in the same cases of Figure 3A, where the negative values have already been modified.

2.3 | Verification of the finite element method model

Firstly, to verify the finite element method (FEM) calculations for the SIF, the obtained results were compared with some results collected from the literature.[30,44]

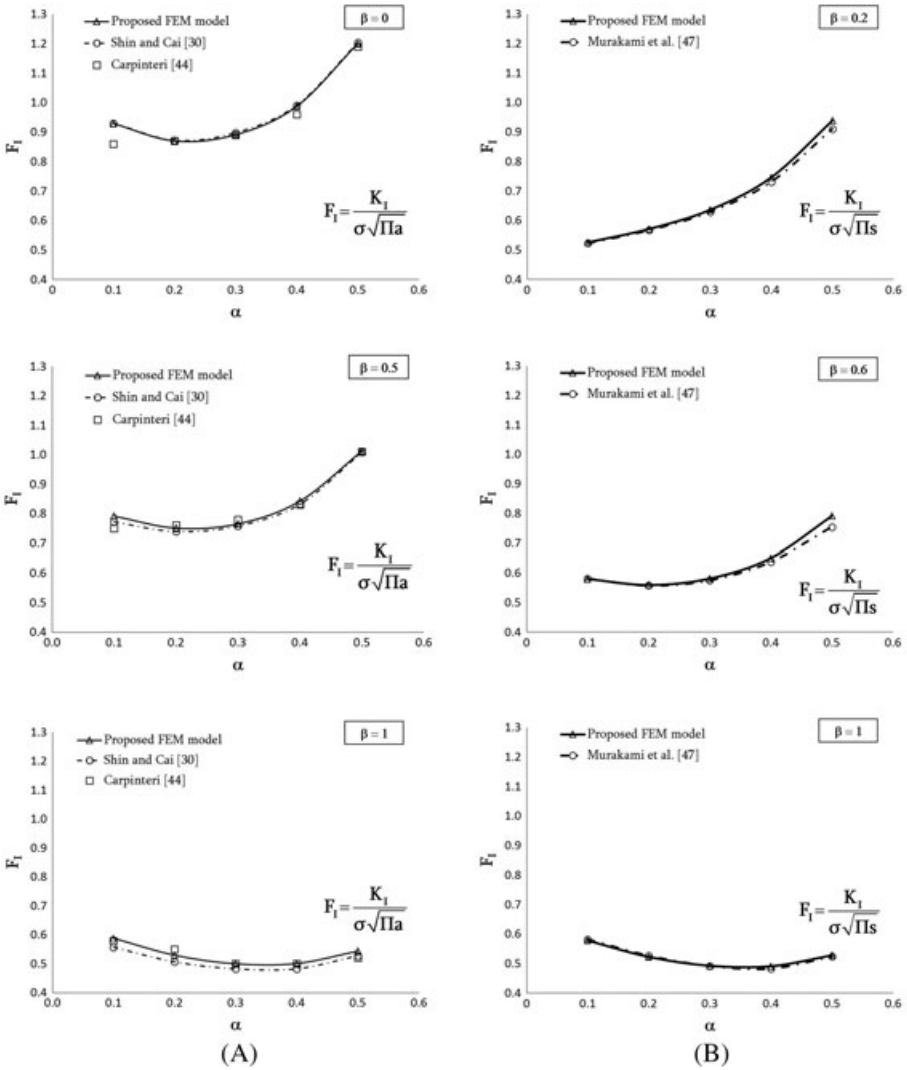

FIGURE 4 Verification of the finite element method (FEM) model. A, Comparison with Shin and Cai[30] and Carpinteri.[44] B, Comparison with Murakami et al[47]

Shin and Cai[30] and Carpinteri[44] developed a numerical model of a shaft under bending, and they studied the SIF along the crack front for different crack geometries. Figure 4A shows the comparison of the SIF results when the crack is completely open at the centre of the crack versus the crack depth α for 3 crack shape factors ($\beta = 0, 0.5, 1$). The results corresponding to other crack shape factors are very similar. We can see a good agreement between the results of the proposed FEM model and the results of Shin and Cai[30] and Carpinteri[44] models. The curves follow the same trend, and the mean relative error is less than 2% in any case.

Secondly, we also verified the proposed FEM model comparing the results with the solutions of Murakami et al,[47] which takes into account the crack shape factor to obtain the nondimensional SIF. Murakami et al[47] determined the nondimensional SIF for a semi-elliptical surface crack in a shaft under bending. The nonsimensional SIF was calculated according to $F_I = \frac{K_I}{\sigma\sqrt{\pi s}}$, where s is the arc COC' (see Figure 1A). Figure 4B shows the comparison of the SIF results at the centre of the crack when the crack is fully open versus the crack depth α for 3 crack shape factors ($\beta = 0.2, 0.6, 1$). In this case, we also can observed a good concordance between both results, and the mean relative error is only about 1.5%

2.4 | Study of the SIF variation during a rotation

In this section, the determination of the SIF using the ABAQUS fracture module was realized for all the aforesaid cases, that is, for all angular positions and for all crack geometries. It was considered that, as said before, if the crack is closed, the values of the SIF are null. For example, the values of the SIF for a crack with $\alpha = 0.4$ and $\beta = 1$ are shown in Figure 5. Each curve shows the evolution of the

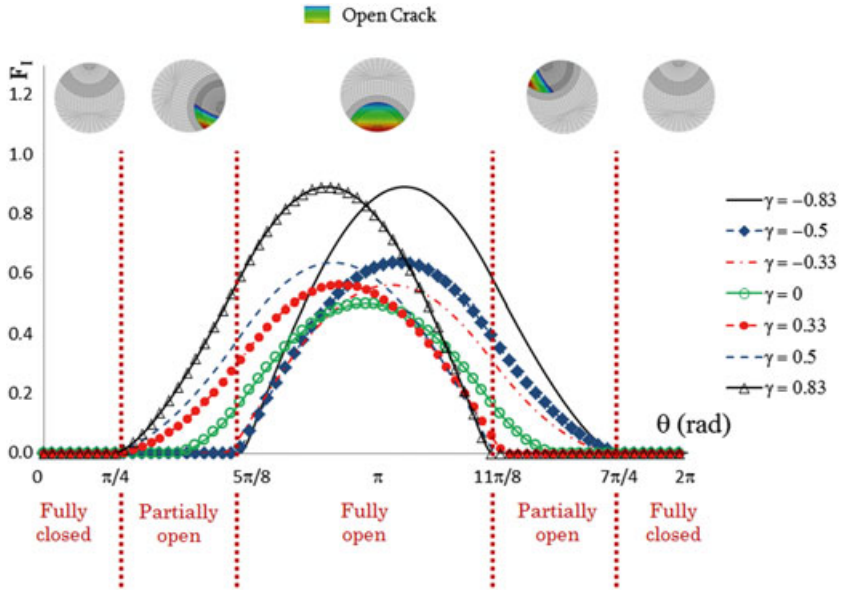

FIGURE 5 Nondimensional stress intensity factor of the finite element method model versus rotation angle, $\beta = 1$ and $\alpha = 0.4$ [Colour figure can be viewed at wileyonlinelibrary.com]

SIF during a rotation for the relative positions on the crack front. We can see that the SIF passes from null to positive values when the crack opens, and then it takes null values when the crack closes again. Between $\theta = 0$ and an angle θ a slightly smaller than $\frac{\pi}{4}$, the crack remains fully closed (the SIF is null in every point of the crack front). When the shaft reaches an angle a slight smaller than $\frac{\pi}{4}$, the crack starts to open, because the SIF is positive in some points and null in other points of the crack front, and remains partially open until $\theta = \frac{5\pi}{8}$. Between $\theta = \frac{5\pi}{8}$ and approximately $\theta = \frac{11\pi}{8}$, the crack is completely open because the SIF is always positive. Finally, in $\theta = \frac{11\pi}{8}$, the crack starts to close again until θ a little bigger than $\frac{7\pi}{4}$, angle in which the crack is completely closed again.

Similarly, in Figure 6, the values of the SIF of a crack with a shape factor $\beta = 0.25$ and 2 depths ($\alpha = 0.2$and0.5) are shown. These results and the ones obtained in Figure 5 can be extended to other crack aspect ratios. The following conclusions can be obtained:

- For the rotation angle $\theta = 0$, the crack is always completely closed, because the SIF is null in every point on the crack front, while for the rotation angle $\theta = \pi$, the crack is always completely open, because the SIF is positive in every point on the crack front, with no dependence on the shape and depth of the crack.
- During one rotation, the crack closes and opens with symmetry, that is to say, the amount of crack that is open is equal for symmetrical rotation angles. For example, if the shaft reaches the rotation angle $\theta = \frac{\pi}{2}$, the part of open crack is equal that for the symmetrical rotation angle $\theta = \frac{3\pi}{2}$.

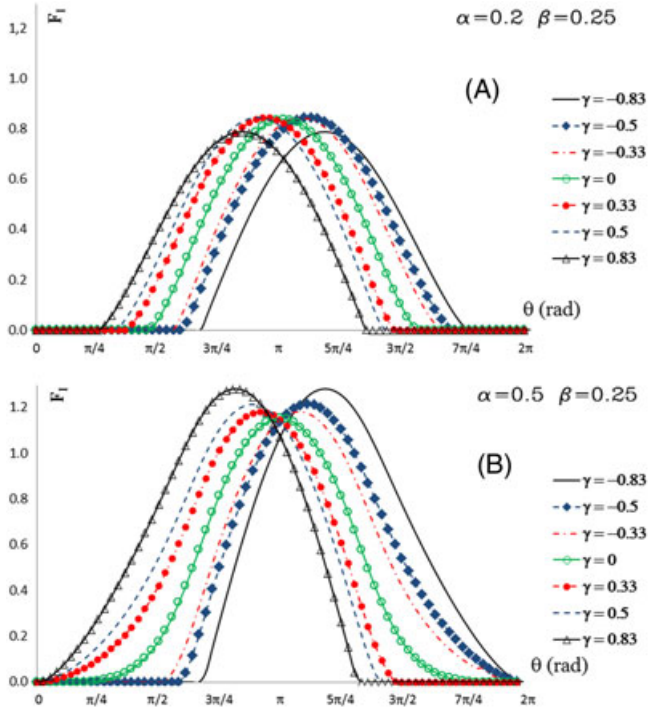

FIGURE 6 Nondimensional stress intensity factor of the finite element method model versus rotation angle. A, $\alpha = 0.2\beta = 0.25$. B, $\alpha = 0.5\beta = 0.25$ [Colour figure can be viewed at wileyonlinelibrary.com]

- The closing time of the crack is proportionally deeper as the crack is longer. In Figure 6, it can be seen that the relative positions in which the SIF is zero for a crack of $\alpha = 0.5$ are lower than for a crack of $\alpha = 0.2$.
- The closing time of the crack is proportionally lower as the crack is longer. In Figure 6, it can be seen that the

relative positions in which the SIF is zero for a crack of $\alpha = 0.5$ are lower than for a crack of $\alpha = 0.2$.

- The opening angle of the crack decreases as the crack depth α increases and the opening angle of the crack increases as the crack shape factor β increases.

3 | ARTIFICIAL NEURAL NETWORK APPROACH

Artificial neural network is a flexible mathematical tool often used to solve different engineering problems because, among others, they are very robust in the case of noisy data and they can be used to identifying complex nonlinear relations between input and output data. An ANN consists of various basic units called neurons, which mimic biological neurons found in living organisms. Each neuron receives several inputs (I_i), from a number of other neurons or external sources. Each input is multiplied by its weight (w_i), one neuron can be accompanied by a threshold parameter called bias (b), and finally, their sums go through an activation function (f) that limits the value of the neuron output (see Figure 7). Hence, the relationship between inputs (I_i) and output (O) can be described as follows:

$$O = f\Big(\sum w_i I_i + b\Big). \tag{4}$$

Neural networks are divided into 3 kinds of layers depending on their positions; these are the input, the output, and the hidden layers. One layer contains one or several neurons. The neurons belonging to the input layer are connected to the external world or the raw data; the hidden layers process the results from the input layer and propagate them to the output layer to achieve the wanted results. In the present work, the multilayer perceptron (MLP) feedword neural network is used. Typically, an MLP neural network contains an input layer, one or several hidden layers, and an output layer, where feedword means that calculations go only from the input layer to the output layer, in one direction. First of all, to establish the weights, a training data that contain a set of input values and the corresponding output values associated with them are required. These data are used by a training process that is based on a learning rule called backpropagation, which learns by the available set of input and output data. In the case of MLP architecture, the backpropagation algorithm is the most common training rule used because it is very efficient and easy to use, especially for complicated data.[48,49] Initially all the edge weights are randomly assigned, and then the ANN is activated and the calculated outputs are compared to the desired outputs; if the difference is above a predetermined threshold, then the weights are adjusted iteratively until the error is below that value. After every iteration, other different couples of inputs and outputs data are used in the neural network validation. During this stage, the neural network performance is evaluated for other unused values. Finally, to confirm the neural network predictive capability, a new set of input and output values are used in the so-called testing phase.

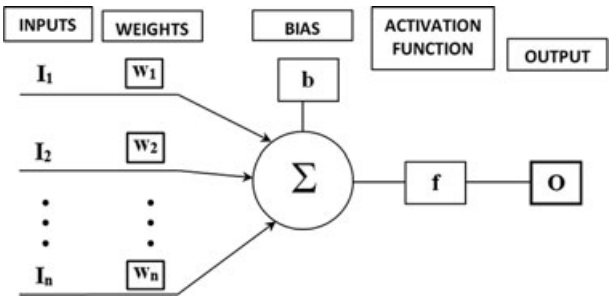

FIGURE 7 Scheme of a single neuron

The method proposed in this work consists of 3 different MLP neural networks. One of them (ANN_1) allows to obtain the first angle during the rotation $\theta_{o\gamma}$, for a known position on the crack front γ, in which F_I is nonzero, that is, the instant when that point located on the crack front opens depends on the relative crack depth α and the crack aspect β. Likewise, the second one (ANN_2) calculates the last angle during the rotation $\theta_{c\gamma}$, for a known position on the crack front γ, in which F_I is positive (the instant when the point closes), it depends also on α and β. Figure 8 shows the nondimensional SIF, F_I, vs rotation angle for a generic crack shape and depth and for a generic location on the crack front, where $\theta_{o\gamma}$ and $\theta_{c\gamma}$ can be found. At last, the third ANN (ANN_3) allows to calculate the dimensionless SIF F_I that for rotating shafts, depends on the crack depth α, the crack aspect β, the relative location along the crack front γ, and the angle of rotation θ. The obtained outputs

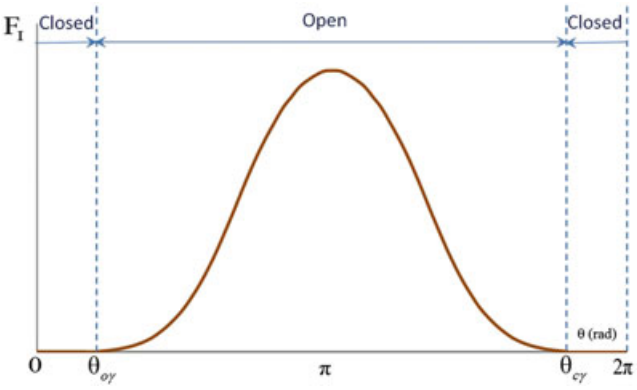

FIGURE 8 Nondimensional stress intensity factor evolution during a rotation for a generic set (α, β, γ) [Colour figure can be viewed at wileyonlinelibrary.com]

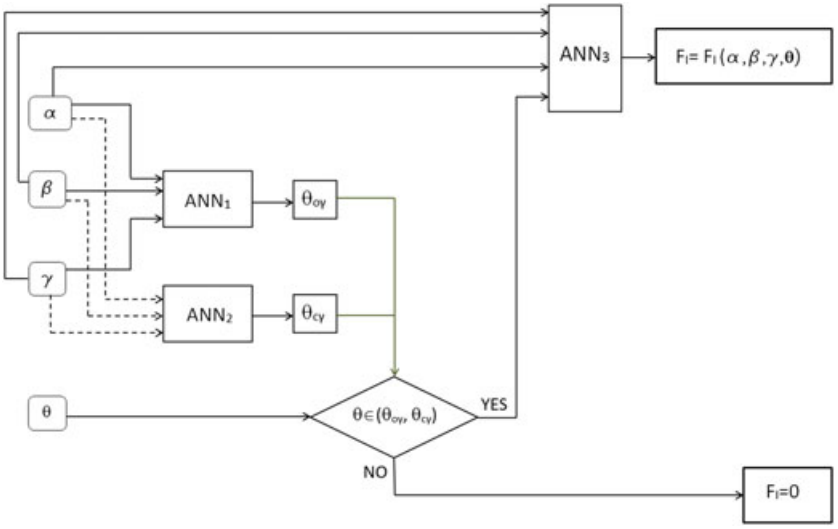

FIGURE 9 Scheme of the proposed method. ANN, artificial neural network [Colour figure can be viewed at wileyonlinelibrary.com]

TABLE 1 Values of R^2 and *MSE* in all cases

	ANN_1		ANN_2		ANN_3	
	R^2	*MSE*	R^2	*MSE*	R^2	*MSE*
Training	0.999	$8.4 \cdot 10^{-4}$	0.999	$8.4 \cdot 10^{-4}$	0.998	$2.8 \cdot 10^{-4}$
Validation	0.996	$1.74 \cdot 10^{-3}$	0.997	$2.44 \cdot 10^{-3}$	0.998	$3.1 \cdot 10^{-4}$

Abbreviations: ANN, artificial neural network; MSE, mean squared error.

from ANN_1 and ANN_2 are used by ANN_3, so that it considers only θ values from $\theta_{o\gamma}$ to $\theta_{c\gamma}$. For values out of the mentioned range, it has been directly assigned $F_I = 0$. In Figure 9, one can see the scheme of the proposed method.

The 3 ANNs used in this work use the *newff* function available in MATLAB to develop a feedforward back propagation network.[50] ANN_1 and ANN_2 have the same structure: 3 inputs in the input layer, in this layer every neuron is connected to one neuron of the first hidden layer, and in the same way, every neuron in the previous hidden layer is connected to one neuron of the next hidden layer. Altogether, one can find 2 hidden layers with 5 neurons per layer. Related to the activation functions, first, to choose the activation functions in the hidden layers it is recommended to use nonlinear activation functions in the case where the ANN has to find a nonlinear relationship between the input and output data, so log-sigmoidal functions were chosen. Second, the linear activation function is used in the output layer because this type of function is suggested for using in estimation problems.[48] At the end, the output layer provides only one output. In the case of ANN_3, its architecture is similar to the previous ones, but one can find 4 inputs in the input layer and 3 hidden layers. In all 3 cases, the ANN bias assignments and initial weights were chosen randomly, and they are updated according to the resilient backpropagation algorithm.

The available data from the numerical model have to be divided into 2 groups to train (first group) and validate (second group) the ANN. The training set consists of 220 data for ANN_1 and ANN_2 and 9000 data for ANN_3, and the validation set consists of 55 data in the case of ANN_1 and ANN_2 and 2528 data for ANN_3. Table 1 shows the minimum mean squared error (MSE) for training and validation data for the presented ANNs according to Equation 5. Finally, the accuracy of the ANN estimations must be checked through R^2 values. Those have been calculated for training and validating steps. They can also be found in Table 1. In all cases, there is very good correlation between actual and predicted values.

$$\begin{aligned} MSE &= \text{Average}[(X_{\text{estimated}} - X_{\text{actual}})^2] \text{ being } X \\ &= F_I, \theta_{o\gamma}, \theta_{c\gamma} \end{aligned} \tag{5}$$

4 | VERIFICATION OF THE PROPOSED METHOD

4.1 | Comparison of numerical and predicted values

To check the goodness of the proposed method, first of all, the values obtained using the neural approach were compared with the data from the numerical model. As an example, Figures 10 and 11 show the F_I values vs the angle of rotation θ for a crack size ratios $\alpha = 0.3$ and $\alpha = 0.5$, respectively, in the case of FEM and ANN results. In each of the graphs, one can see the curves that

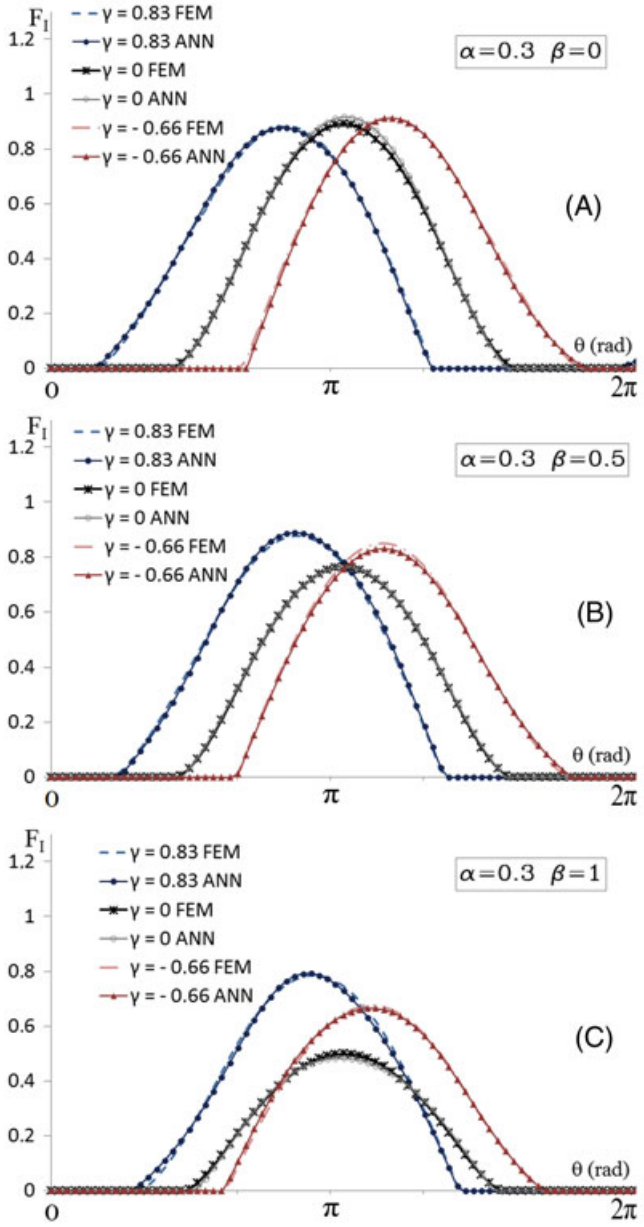

FIGURE 10 ANN results and numerical ones vs revolution angle. A, $\alpha = 0.3\beta = 0$. B, $\alpha = 0.3\beta = 0.5$. C, $\alpha = 0.3\beta = 1$. ANN, artificial neural network; FEM, finite element method [Colour figure can be viewed at wileyonlinelibrary.com]

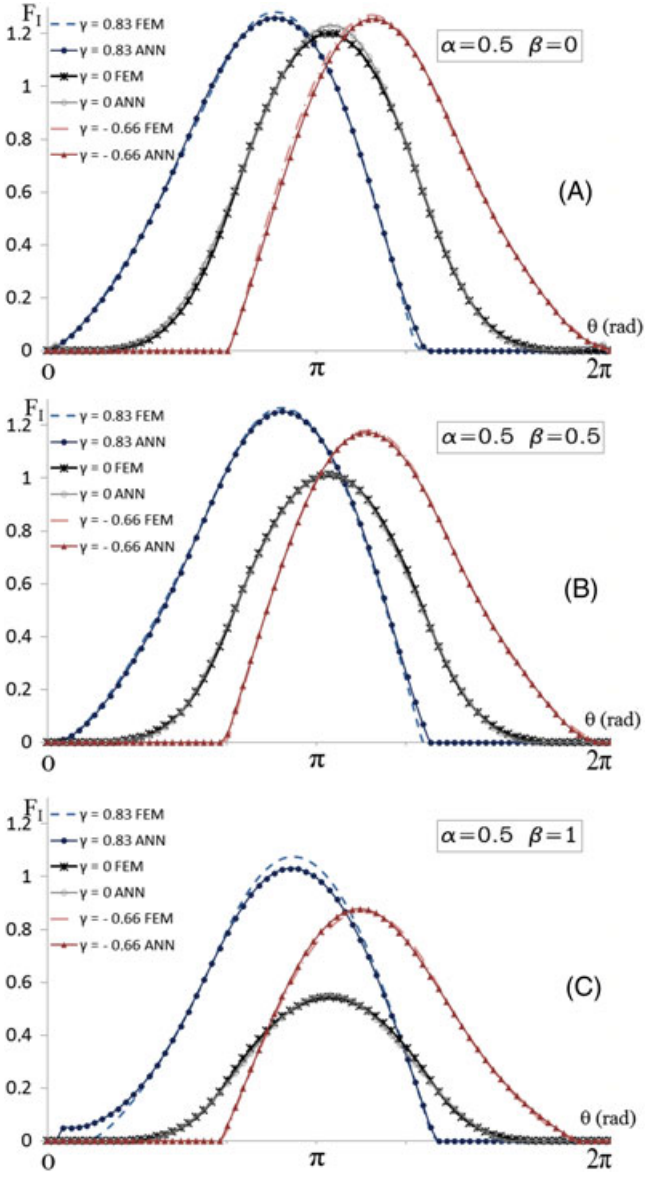

FIGURE 11 ANN results and numerical ones vs revolution angle. A, $\alpha = 0.5\beta = 0$. B, $\alpha = 0.5\beta = 0.5$. C, $\alpha = 0.5\beta = 1$. ANN, artificial neural network; FEM, finite element method [Colour figure can be viewed at wileyonlinelibrary.com]

represent the dimensionless SIF evolution at several positions on the crack front during a revolution for several cases of β (0, 0.5, and 1) and γ (−0.83, −0.66, 0, 0.66, and 0.83). The results corresponding to other crack geometries and other positions on the front are similar to the ones that are shown.

As can be seen, most of the results obtained from the ANNs method are very similar to the numerical ones; the discrepancies between both data sets increase for circular large depths near $\alpha = 0.5$ at crack ends. This may be due to the crack ends are problematic zones because in the intersection points the singularity power depends on the intersection angle and Poisson's ratio and it is not −1/2. However, the maximum error is only about 4%. Moreover, circular crack fronts are rare shapes. If other crack shapes, sizes, and locations on the crack front are analysed, the results are similar to the ones previously shown. In addition, Figure 12 shows the residuals, calculated as the difference between the numerical nondimensional SIF value and the estimated one, with respect to estimated nondimensional SIF F_I, as can be seen, virtually all of the points follow a random pattern, so that residuals are smaller for middle values in the graphs and they increase at limit values, but their absolute values do not exceed 0.09.

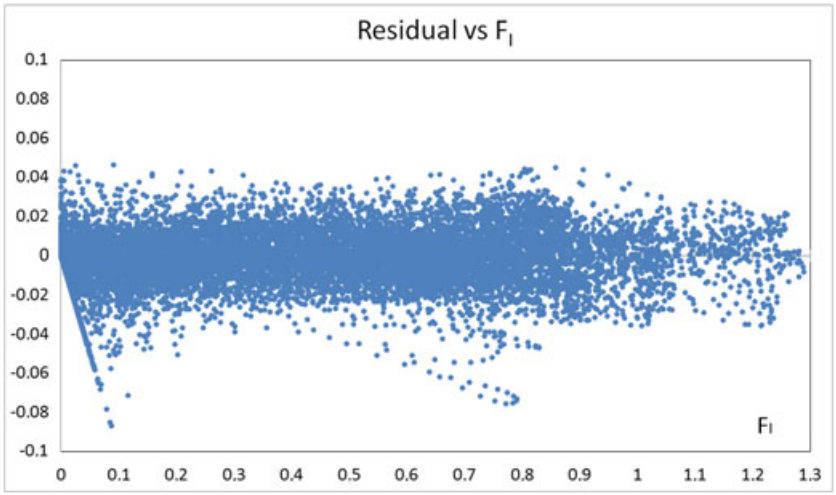

FIGURE 12 Residual vs estimated F_I with the artificial neural networks [Colour figure can be viewed at wileyonlinelibrary.com]

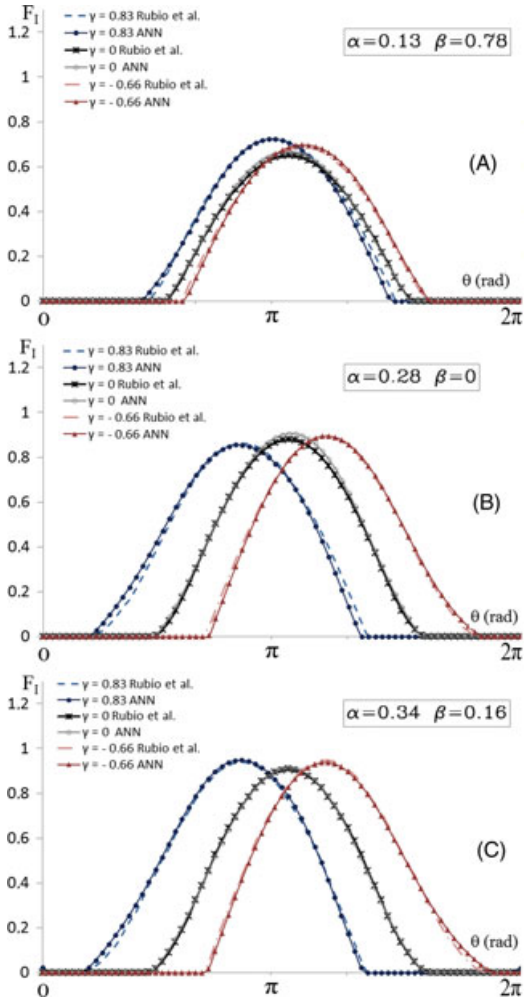

FIGURE 13 Comparison of the artificial neural networks (ANNs) results with Rubio et al.[34] A, $\alpha = 0.13\beta = 0.75$. B, $\alpha = 0.28\beta = 0$. C, $\alpha = 0.34\beta = 0.16$ [Colour figure can be viewed at wileyonlinelibrary.com]

4.2 | Verification of the model

Finally, to verify the proposed method, some results of the obtained nondimensional SIF by the present method were compared with others from the expression developed by Rubio et al, which can be found in previous study.[34] Three cases have randomly been chosen: ($\alpha = 0.13$, $\beta = 0.78$), ($\alpha = 0.28$, $\beta = 0$), and ($\alpha = 0.34$, $\beta = 0.16$). Figure 12 shows the nondimensional SIF evolution for these 3 samples at several positions on the crack front during a rotation. These crack configurations were not used for training the ANNs.

As can be seen, the comparison shows good agreement between the reference[34] and estimated (proposed method) values. These results are especially good in the case of small and medium depths ($\alpha = 0.13$, $\beta = 0.78$) and ($\alpha = 0.28$, $\beta = 0$), when crack depth increases the estimation results becomes slightly worse, regardless of the crack aspect ratio. Maximum, minimum, and medium residual values for each of the 3 cases can be seen in Table 2, taking into account all the positions along the crack front and the rotation angles. In most observations, residual values are less than 0.01; these differences are comparable with the residuals of similar cases collected in previous sections. The larger differences between reference and estimated data (0.162) are found in the case $\alpha = 0.47$, $\beta = 0.38$; examining these graphs one can see that estimated curves are similar to the reference ones but they are slightly displaced

TABLE 2 Maximum, minimum, and medium residual values

	$\alpha = 0.13$, $\beta = 0.78$	$\alpha = 0.28$, $\beta = 0$	$\alpha = 0.34$, $\beta = 0.16$
Maximum residual	0.058	0.078	0.053
Minimun residual	−0.034	−0.054	−0.046
Medium residual	−0.002	−0.003	0.001

to the left; it means that $\theta_{o\gamma}$ and $\theta_{c\gamma}$ estimations are smaller than the actual values (about 5%) but the rate of open crack for a given γ along a rotation is equal in both cases.

5 | CONCLUSIONS

In this study, a methodology, founded on ANNs, that estimates the values of the SIF at the crack front for a rotating cracked shaft taking into account the crack depth, the crack shape, the point location on the crack front, and the angle of rotation was developed. The necessary data to train the ANN were obtained from a 3D quasi-static finite element model of a shaft, which is subjected to rotary bending loads. Regarding the proposed method, it was designed until the estimation results present a very good agreement with the offered by the numerical model and, later, it was checked by comparison with results by others authors found in the literature. The comparison shows good agreement between the reference values and the estimated ones, especially good in the case of small and medium depths. The obtained results show that the neural approach is effective to estimate SIF values in rotating cracked shafts assuming elliptical cracks. The formulation of the proposed ANN method would allow studying the complex dynamic performance of cracked shafts to predict the remaining life of the element analysing the propagation of cracks contained in rotating shafts by means of the Paris Law considering the nonlinear behaviour of the shaft.

ACKOWLEDGEMENT

The authors would like to thank the Spanish Ministerio de Economía y Competitividad for the support for this work through the projects DPI2009-13264 and DPI2013-45406-P

REFERENCES

1. Papadopoulos CA, Dimarogonas AD. Coupled longitudinal and bending vibrations of a rotating shaft with an open crack. *J Sound Vib*. 1987;117(1):81-93.
2. Papadopoulos CA, Dimarogonas AD. Coupled longitudinal and bending vibrations of a cracked shaft. *J Vibration, Acoustics, Stress and Reliability in Design*. 1988;110:1-8.
3. Gasch R. A survey of the dynamic behavior of a simple rotating shaft with a transverse crack. *J Sound Vib*. 1993;160:313-332.
4. Gasch R. Dynamic behaviour of the laval rotor with a transverse crack. *Mech Syst Sig Process*. 2008;22:790-804.
5. PC Müller DSöffker J. Bajkowski. Chaotic motions and fault detection in a cracked rotor. *Nonlinear Dyn*. 1994;5(2):233-254.
6. Pu YP, Chen J, Zhong P. Quasi-periodic vibration of cracked rotor on flexible bearings. *J Sound Vib*. 2002;251(5):875-890.
7. Qin WY, Chen G, Ren X. Grazing bifurcation in the response of cracked Jeffcott rotor. *Nonlinear Dyn*. 2004;35(2):147-157.
8. Qin WY, Meng G, Zhang T. The swing vibration, tranverse oscillation of cracked rotor and the intermittence chaos. *J Sound Vib*. 2003;259(3):571-583.
9. Al-Shudeifat MA, Butcher EA. New breathing functions for the transverse breathing crack of the cracked rotor system: approach for critical and subcritical harmonic analysis. *J Sound Vibr*. 2011;303(3):526-544.
10. Bachschmid N, Pennacchi P, Tanzi E. Some remarks on breathing mechanism, on non-linear effects and on slant and helicoidal cracks. *Mechanical Syst Sig Process*. 2008;22:879-904.
11. Darpe AK. A novel way to detect transverse surface crack in a rotating shaft. *J Sound Vib*. 2007;305(1–2):151-171.
12. Darpe AK, Gupta K, Chawla A. Coupled bending, longitudinal and torsional vibrations of a cracked rotor. *J Sound Vib*. 2004;269(1-2):33-60.
13. Darpe AK, Gupta K, Chawla A. Transient response and breathing behaviour of a cracked Jeffcott rotor. *J Sound Vib*. 2004;272:207-243.
14. Jun OS, Eun HJ, Earmme YY, Lee CW. Modelling and vibration analysis of a simple rotor with a breathing crack. *J Eng Mech*. 1992;155(2):273-290.
15. Keiner H, Gadala MS. Comparison of different modelling techniques to simulate the vibration of a cracked rotor. *J Sound Vib*. 2002;254(5):1012Ű-1024.
16. Mayes IW, Davies WGR. Analysis of the response of a multi-rotor-bearing system containing a transverse crack in a rotor. *J Vibration, Acoustics, Stress, and Reliability in Design*. 1984;106(1):139-145.
17. Patel TH, Darpe AK. Influence of crack breathing model on nonlinear dynamics of a cracked rotor. *J Sound Vib*. 2008;311:953-972.
18. Sinou JJ, Lees AW. The influence of cracks in rotating shafts. *J Sound Vib*. 2005;285:1015-1037.
19. Tsai TC, Wang YZ. Vibration analysis and diagnosis of a cracked shaft. *J Sound Vib*. 1996;192(3):607-620.
20. Yang B, Suh CS. On fault induced nonlinear rotary response and instability. *Int J Mech Sci*. 2006;48:1103-1125.
21. Blackburn WS. Calculation of stress intensity factors for straight cracks in grooved and ungrooved shafts. *Eng Fract Mech*. 1976;8(4):731-736.
22. Bush AJ. Experimentally determined stress-intensity factors for single-edge-crack round bars loaded in bending. *Exp Mech*. 1976;16(7):249-257.
23. Carpinteri A. Stress intensity factors for straight-fronted edge cracks in round bars. *Eng Fract Mech*. 1992;42(6): 1035-1040.
24. Ouchterlony F. Extension of the compliance and stress intensity formulas for the single edge crack round bar in bending. In: Freiman SW, Fuller ER, eds. *Fracture Mechanics Methods for Ceramics, Rocks, and Concrete*, American Society for Testing and Materials. Pa: Philadelphia; 1981:237-256.
25. Valiente A. Criterios de fractura para alambres, thesis doctoral, Universidad Politecnica de Madrid (In Spanish).
26. Astiz MA. An incompatible singular elastic element for two- and three-dimensional crack problems. *I J Fract*. 1986;31(2): 105-124.

27. Couroneau N, Royer J. Simplified model for the fatigue growth analysis of surface cracks in round bars under mode i. *Int J Fatigue*. 1998;10:711-718.
28. Levan A, Royer J. Part-circular surface cracks in round bars under tension, bending and twisting. *Int J Fract*. 1993;61(1):71-99.
29. Shih YS, Chen JJ. Analysis of fatigue crack growth on a cracked shaft. *Int J Fatigue*. 1997;19(6):477-485.
30. Shin CS, Cai CQ. Experimental and finite element analyses on stress intensity factors of an elliptical surface crack in a circular shaft under tension and bending. *Int J Fract*. 2004;129:239-264.
31. Yang FP, Kuang ZB. Stress intensity factors for surface fatigue crack in a round bar under cyclic axial loading. *Fatigue Fract Eng Mater Struct*. 2007;30(7):621-628.
32. Carpinteri A, Brighenti R, Spagnoli A. Surface flaws in cylindrical shafts under rotary bending. *Fatigue Fract Eng Mater Struct*. 1998;21:1027-1035.
33. Dao NH, Sellami H. Stress intensity factors and fatigue growth of a surface crack in a drill pipe during rotary drilling operation. *Eng Fract Mech*. 2012;96:626-640.
34. Rubio P, Rubio L, Munoz-Abella B, Montero L. Determination of the stress intensity factor of an elliptical breathing crack in a rotating shaft. *Int J Fatigue*. 2015;77:216-231.
35. Hasanzadehshooiili H, Lakirouhani A, Sapalas A. Neural network prediction of buckling load of steel arch-shells. *Archives of Civil and Mech Eng*. 2012;22(4):477-484.
36. Heng A, Zhang S, Tan ACC, Mathew J. Rotating machinery prognostics: state of the art, challenges and opportunities. *Mech Syst Sig Process*. 2009;23:724-739.
37. Munoz-Abella B, Rubio L, Rubio P. Stress intensity factor estimation for unbalanced rotating cracked shafts by artificial neural networks. *Fatigue Fract Eng Mater Struct*. 2015;38(3):352-367.
38. Nazari A. Application of artificial neural networks for analytical modeling of Charpy impact energy of functionally graded steels. *Neural Comput Appl*. 2013;22:731-745.
39. Sekhar AS. Multiple cracks effects and identification. *Mech Syst Sig Process*. 2008;22:845-878.
40. Srinivas HK, Srinivasan KS, Umesh KN. Role of artificial neural network and a wavelet transform for condition monitoring of the combined faults of unbalance and cracked rotors. *Int J Acoust Vibr*. 2010;15(3):121-127.
41. Youngho K, Junyoung JK, Wanjo R, Dong-Whan C. Multiple defect diagnostics of gas turbine engine using SVM and RCGA-based ANN algorithms. *J Mech Sci Technol*. 2012;26(5):1623-1632.
42. Deng J, Mao H. A blank optimization design method for three-roll cross rolling of complex-groove and small-hole ring. *Int J Mech Sci*. 2015;93:218-228.
43. Ba~ant ZP, Estenssoro LF. Surface singularity and crack propagation. *Int J Solids Struct*. 1979;15(5):405-426.
44. Carpinteri A. Elliptical-arc surface cracks in round bars. *Fatigue Fract Eng Mater Struct*. 1992;15:1141-1153.
45. Carpinteri A, Brighenti R. Part-through cracks in round bars under cyclic combined axial and bending loading. *Int J Fatigue*. 1996;18:33-39.
46. ABAQUS. Abaqus Theory Manual, Version 6.7. Dassault Systèmes Inc; 2007.
47. Murakami Y. *Stress Intensity Factors Handbook*. Oxford: Pergamom Press; 1986;654-667.
48. Haykin S. *Neural Networks: A Comprehensive Foundation*. Ontorio: Prentice Hall; 1999.
49. Khotanzad A, Chung C. Application of multi-layer perceptron neural networks to vision problems. *Neural Comput Appl*. 1998;7:249-259.
50. Neural Network Toolbox UserŠs Guide. *MATLAB TM*.